J. Fluid Mech. (1986), *vol.* 164, *pp.* 449–467
Printed in Great Britain

Measurements of lift in oscillatory flow

By G. N. ROSENTHAL† AND J. F. A. SLEATH
Department of Engineering, University of Cambridge

(Received 26 June 1985)

Measurements are reported of the lift on a sphere in oscillatory flow. Two different oscillating-tray rigs were used and measurements were made for a sphere at various distances from both smooth and rough beds. For the rough bed, the roughness consisted of a single close-packed layer of similar spheres glued to the surface of the tray. Both smooth and rough beds showed somewhat similar trends. At sufficiently low Reynolds numbers the lift varied smoothly during the course of the cycle with maxima near the point at which fluid velocity was greatest and minima near velocity reversal. However, at higher Reynolds numbers a secondary peak began to appear near the point of velocity reversal. It is suggested that this secondary peak may be associated with vortex formation around the sphere. When the sphere diameter D was large compared with the viscous-boundary-layer lengthscale $1/\beta$ ($= (2\nu/\omega)^{\frac{1}{2}}$), the maximum value of C_L during the course of a half-cycle initially increased with increasing Reynolds number, reached a maximum, and then declined steadily. The curves were similar for smaller βD-values except that the tests did not extend to low enough Reynolds numbers to show the initial rise. For the smaller values of βD the lift record became unstable when the Keulegan–Carpenter number exceeded approximately 244. At higher βD-values it was not possible to observe any significant instability for the range of Reynolds numbers investigated.

1. Introduction

This paper describes an experimental investigation of the lift on spheres near both plane and rough walls in oscillatory flow. The original motivation for this study was to try to shed some light on the problem of sediment transport. It seems probable that lift forces are important for the transport of particles of sediment both in suspension and as bed load but there are still significant gaps in our knowledge of how lift varies with Reynolds number and distance from the bed. This is particularly true of oscillatory flow.

A potential-flow solution for the lift on a sphere near a plane wall has been obtained by Milne Thomson (1968). This solution is a first approximation valid for small values of the ratio of sphere diameter D to gap ϵ between the sphere and the wall. A second approximation was derived by Naheer (1977). Low-Reynolds-number steady-flow solutions have been obtained by Rubinow & Keller (1961) for the case of a spinning sphere moving through an unbounded viscous fluid and by Saffman (1965, 1968) for an isolated sphere in an unbounded shear flow. More recently, Auton (1984) has carried out an inviscid analysis for the lift on a sphere in a shear flow.

There have been several experimental investigations of the lift on spheres in steady flow (e.g. Young 1960; Chepil 1961; Swanson 1961; Coleman 1967; Willmarth &

† Present address: Department of Civil Engineering, University of Cape Town.

Enlow 1969; Thomschke 1971; Chen & Carstens 1973; Aksoy 1973; Bagnold 1974; Davies & Samad 1978; Lee 1979; and Willetts & Murray 1981) but there has been surprisingly little work on oscillatory flow. As far as the writers are aware, the only direct measurements of lift on spheres in oscillatory flow are those contained in an unpublished thesis by Sert (1977). Unfortunately, these cover only a limited range and suffer from some experimental problems which will be discussed below.

There have, however, been several measurements of lift in oscillatory flow for cylinders (Sarpkaya 1976; Maull & Norman 1978; Maull & Milliner 1978). Although these results are not directly comparable with those of the present paper, because of the difference between flows round two- and three-dimensional bodies and also because most of the cylinder results are for much larger Reynolds numbers, the general trends may be qualitatively similar.

For the purposes of the present paper lift is taken to be the force acting vertically away from the bed. Sideways forces (i.e. parallel to the bed and perpendicular to the flow) are not investigated here.

2. Experimental arrangement and method

One of the problems with measurements in oscillatory flow is that the lengthscale of the viscous boundary layer is extremely small. Since this lengthscale is proportional to the square root of kinematic viscosity it was decided to use air rather than water as the working fluid.

Measurements were made with two different rigs. The first consisted of the apparatus shown schematically in figure 1. In this apparatus, which will be referred to as the 'oscillating-tray rig', a flat tray was oscillated backwards and forwards in its own plane by a Scotch-yoke mechanism driven by a variable-speed motor with feedback control. The other rig, which will be referred to as the 'pendulum rig', is shown schematically in figure 2. It consisted essentially of a tray, suspended from the roof, which was free to swing backwards and forwards at its natural frequency. Each rig had advantages and disadvantages. The oscillating-tray rig could be driven over a wide range of frequencies of oscillation. On the other hand, it was more prone to vibration problems and could not easily be driven at very large amplitudes. The pendulum rig did not suffer from vibration problems and could attain much larger amplitudes but was limited to periods of oscillation T of about 4.3 s.

In the oscillating-tray rig the tray slid on continuously lubricated V-section rails. Teflon bearing pads were used to reduce friction. To minimize vibration the motor and Scotch yoke were mounted separately from the oscillating-tray assembly. Great care was taken to ensure accurate alignment of the drive mechanism and rails. As a further precaution, an Euler strut capable of restricted flexing was inserted in the drive shaft.

For the experiments with an isolated sphere near a smooth bed, the upper surface of the tray consisted of a flat horizontal Dural plate of length 1.37 m and breadth 0.30 m. Each end of this plate was hinged to a similar horizontal plate of breadth 0.30 m. At the drive end the extension plate was 0.60 m long and the other was 0.87 m long. These extension plates slid on felt pads over the horizontal surface of the tray housing. The effect of this arrangement was to mimimize leakage of air from beneath the tray into the closed chamber above the flat plate.

The tray of the pendulum rig was 0.30 m wide and approximately 5 m long. The upper surface had a radius of curvature of 5 m and the height of the supporting hinge above the tray was also 5 m. For the smooth-bed tests the upper surface of the tray

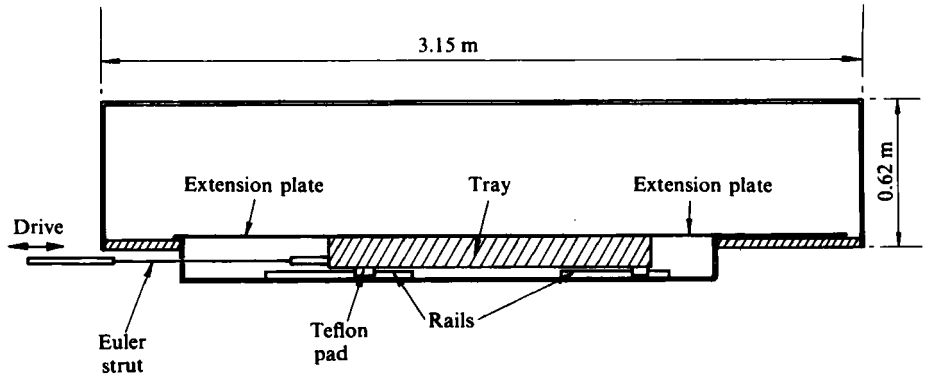

FIGURE 1. The oscillating-tray rig.

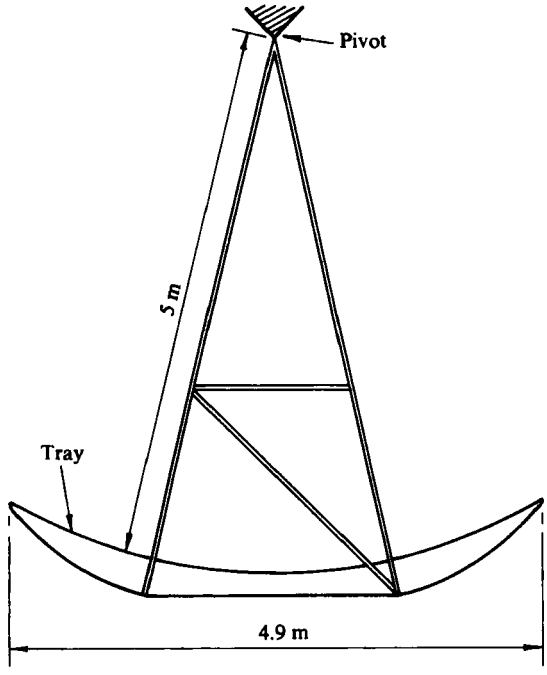

FIGURE 2. The pendulum rig.

consisted of varnished plywood except for the top of the force-transducer housing, which was made of Dural and was 0.30 m long × 0.18 m wide. The upper surface of the tray was shielded from draughts by means of a plywood housing. It had originally been intended to support the tray from the pivot by means of piano wire. However, problems were encountered with parasitic oscillations of the tray and consequently the wires were replaced by a rigid steel frame.

The transducer used to measure the lift force on the sphere was the same for each rig. The sphere was mounted on the end of a vertical steel rod which poked up through a 2.5 mm diameter hole in the tray. The leakage of air through this hole was restricted by carefully sealing the transducer housing to the underside of the tray. The rod was supported by two pretensioned cruciform foils as shown in figure 3. The foils were made of stainless steel and were 0.15 mm thick. Semi-conductor strain gauges were

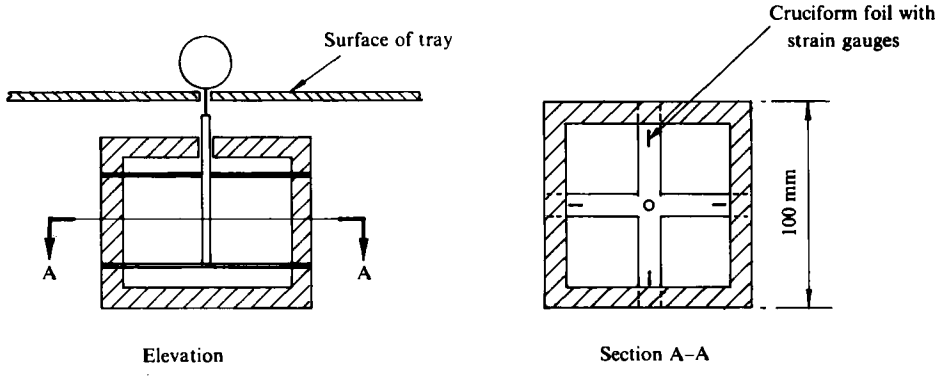

FIGURE 3. The force transducer.

glued to the arms of the lower foil. The gauges were connected across an a.c. Wheatstone bridge and the out-of-balance signal was passed directly, through a Krohn–Hite active filter, a Racal Store 7 recorder amplifier and an analog-to-digital converter, to a computer for analysis. This particular support system was chosen because of its stiffness (deflections of the sphere during the course of a cycle of oscillation were typically only a few micrometres) and also because the out-of-balance signal from the gauges is most sensitive to vertical force on the sphere. It was originally expected that, despite this arrangement, there would still be considerable influence of the in-line force on the out-of-balance signal. It was with the intention of applying a correction for the in-line force that gauges were fixed to all four arms of the foil. However it was found that, using the output only from the gauges on the arms aligned at right angles to the direction of oscillation and making use of the experimental procedure outlined below, the contributions of in-line force and horizontal sideways force to the final output were negligible.

Calibration of the transducer was carried out before and after each test by placing and removing known weights on top of the sphere being tested. Figure 4 shows a typical calibration curve.

The experimental procedure was as follows. For the oscillating-tray rig the required amplitude and frequency of oscillation were selected and the rig was left running until the flow conditions had become stable. The measuring equipment was left on day and night and consequently did not require a warm-up period. Measurements were then made with an airtight box placed over the sphere. Output from a phase marker attached to the drive shaft of the motor was also fed into the computer. Next, the airtight box was removed and the measurements repeated with the sphere exposed to the flow. Finally, the box was replaced and the measurements repeated again. This last measurement was to ensure that there had been no drift in the output signal from that at the beginning of the test. Although the semiconductor gauges were carefully matched to minimize temperature effects, some difficulty was experienced with drift when conditions in the laboratory were changing rapidly.

The experimental procedure for the tests with the pendulum rig was very similar. The only significant difference was that the flow could not be left quite so long to settle down because of the gradual decrement in amplitude of oscillation. This could have been avoided by forcing the oscillation of the pendulum but it was decided that the advantages of extremely low vibration outweighed the disadvantage of slight variation in amplitude. The normal procedure was for the pendulum to be gently drawn back beyond the required amplitude and then released. The pendulum was

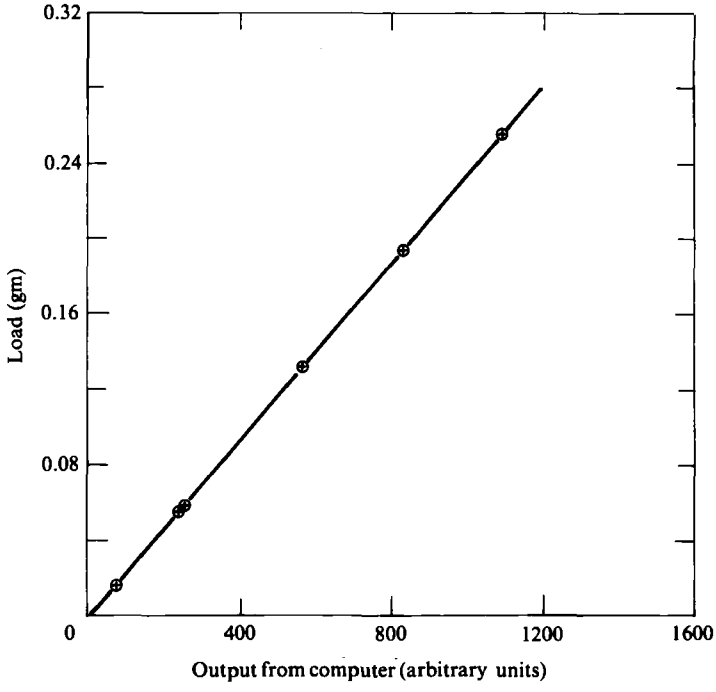

FIGURE 4. Typical calibration curve.

then allowed to swing freely until the amplitude decayed to the required value and measurements were started. This critical amplitude was detected with the aid of a stationary light source and photo-electric cell activated by a reflective strip attached to the tray. Normally, the pendulum completed five or six cycles before readings were started. The change in amplitude of oscillation from one cycle to the next did not exceed 0.8 % of the amplitude. Otherwise, the test procedure was the same as for the oscillating tray rig.

The lift signal was obtained as the difference between the output with the sphere exposed to the flow and that with the airtight box in place. A number of examples of the resulting signal are shown in figure 5. In this figure U_0 is the amplitude of the tray velocity, ν is kinematic viscosity and $\beta = (\omega/2\nu)^{\frac{1}{2}}$, where ω is the angular frequency of oscillation. The lift has been expressed in terms of the lift coefficient

$$C_{\mathrm{L}} = \frac{\text{lift}}{\frac{1}{2}\rho U_0^2(\frac{1}{4}\pi D^2)},$$

where ρ is fluid density. Phase is taken to be zero at the moment when the velocity of the tray reverses and the tray velocity is maximum at phases of $\frac{1}{2}\pi$ and $\frac{3}{2}\pi$.

By symmetry, the lift during one half-cycle should be the same as that during the next, unless subharmonics caused by preferential vortex shedding are significant. On the other hand, the in-line force is equal and opposite during one half-cycle to that during the other. The fact that the records shown in figure 5 are almost the same from one half-cycle to the next provides confirmation that the contribution of the in-line force to the final signal is indeed small.

The Krohn–Hite filter was operated in low-pass mode. For the oscillating-tray tests the cutoff frequency was 30 times the frequency of oscillation. The filter was not strictly necessary for the pendulum-rig tests but was used in order to maintain

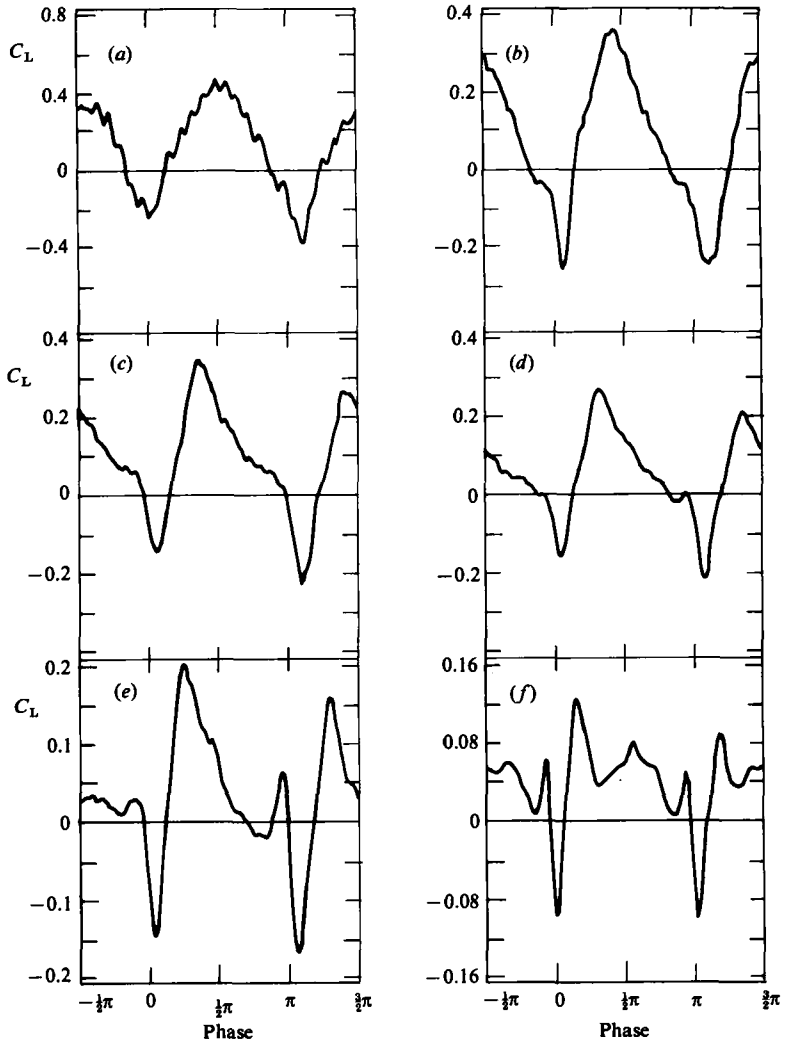

FIGURE 5. Examples of the way in which the lift coefficient varies in the pendulum rig during the course of the cycle. The values of $U_0 D/\nu$ are: (*a*), 922, (*b*) 1227, (*c*) 1534, (*d*) 1840, (*e*) 2454, (*f*) 4908. In each case $\beta D = 14.0$, $\epsilon/D = 0.375$, $D = 63.9$ mm.

comparability with the other tests; the cutoff frequency was 7 Hz for the tests discussed in this paper. Since the highest frequencies of oscillation were 1.1 Hz for the oscillating tray and 0.23 Hz for the pendulum, the amplitude attenuation of the signal was negligible except, possibly, for the spike in the record near velocity reversal which is discussed below. However, the effect on phase was more significant. For the measurements shown in figure 5 the phase shift was found to be 20.2°. The records in figure 5 have been corrected for this shift.

In the rough-bed tests the trays were covered with a single layer of spheres, of the same diameter D as that being tested, in a close-packed array. At right angles to the direction of oscillation the distance between sphere centres was equal to $D\sqrt{3}$, whereas in the direction of oscillation the distance between centres was D. In most tests no attempt was made to fill the space under the sphere attached to the transducer when it was raised above the bed. However, when the distance of the

βD	Apparatus	D (mm)	Range of $U_0 D/\nu$
	Smooth bed		
18	Oscillating tray	38	700–2400
16.9–17.0	Pendulum	76.2	750–6000
14	Oscillating tray	38	250–2000
14.0–14.1	Pendulum	63.9	300–5000
11.1	Pendulum	51	480–3900
10	Oscillating tray	38	700–1000
8.2–8.4	Pendulum	38	360–3000
4.1–4.3	Pendulum	19	180–1835
2.8	Pendulum	12.7	246–1096
1.3–1.4	Pendulum	6.12	231–537
	Rough bed		
8.3	Pendulum	38	360–3000
4.2	Pendulum	19	200–1500
2.1	Pendulum	9.5	360–900

TABLE 1. Summary of test conditions

sphere from the bed was equal to D some tests were carried out with a dummy sphere inserted below it.

Measurements of air temperature, pressure and relative humidity were made before and after each test. The range of tests carried out is shown in table 1. All of the spheres were smooth.

3. Test results and discussion

3.1. *Smooth beds*

A first question which has to be answered is whether the two rigs give comparable results under similar flow conditions. It might be thought, for example, that the curvature of the flow in the case of the pendulum rig would affect the results. Direct comparison is not entirely straightforward because the operating ranges of the two rigs were different and, where they did overlap, experimental errors were not insignificant. However, figure 6 shows a typical comparison. We see that the overall shape of the curves is very similar in the two cases although in figure 6(*b*) it looks as if there has been a slight shift in the origin of C_L, perhaps due to temperature drift. However, the fact that the Reynolds numbers were not quite the same in figure 6(*b*) may have affected the comparison. Bearing in mind that a value of $C_L = 0.1$ corresponds to a lift force of only 39 μN in figure 6(*b*) the agreement is reasonably satisfactory. It should also be pointed out that the sphere in the pendulum rig was almost twice as large (cf. table 1) as that in the oscillating tray and was close to the maximum diameter tested. The reasonable agreement between the results from the two rigs suggests that sidewall effects were not significant. This conclusion was supported by the results of other tests. Since the ratio of sting to sphere diameter also varied by a factor of about two it would seem that the influence on the results of the sting supporting the spheres was not significant either. As in figure 5, a correction for the phase shift introduced by the filter has been applied.

Figure 7 shows how the lift coefficient varies with Reynolds number and gap ratio

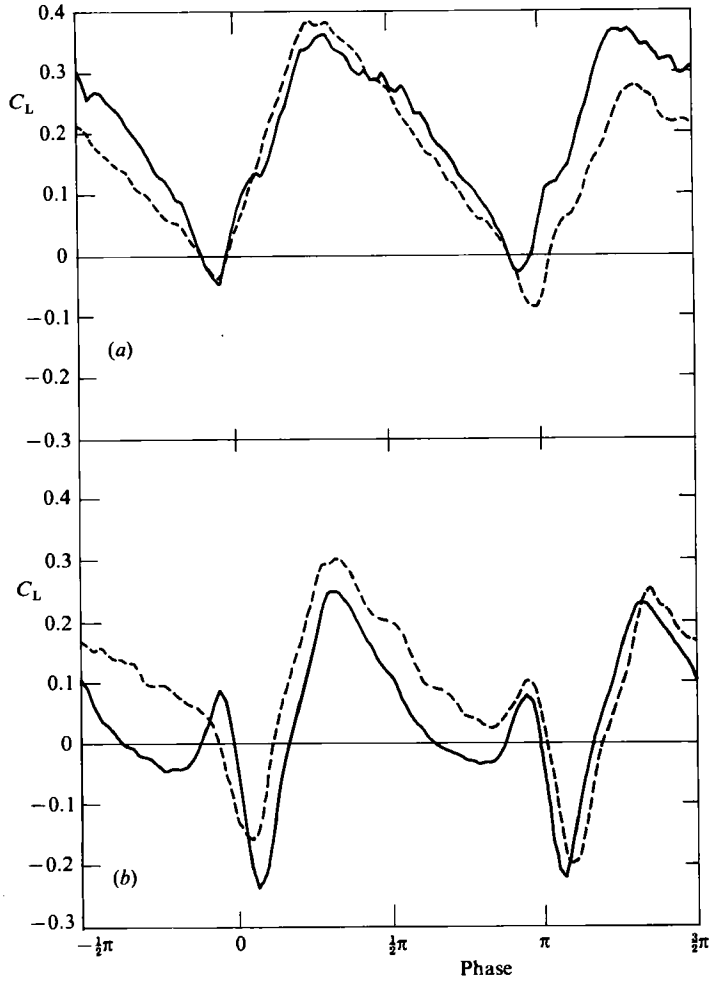

FIGURE 6. Comparison between the results obtained in the oscillating-tray rig (solid lines) and the pendulum rig (dashed lines) for $\beta D = 14.0$. (*a*) $\epsilon/D = 0.0156$, $U_0 D/\nu = 2000$ (tray) and 1997 (pendulum); (*b*) $\epsilon/D = 0.25$, $U_0 D/\nu = 1900$ (tray) and 1840 (pendulum).

ϵ/D. In this case $\beta D = 14$, which means that the sphere is very large compared with the lengthscale $1/\beta$ of the viscous oscillatory boundary layer. The curves for the amplitude of the lift coefficient and for the maximum positive lift coefficient (away from the bed) show a similar pattern: as Reynolds number increases from zero, C_L rises to a maximum and then decreases again. The curves in figure 7(*c*) for the maximum negative lift coefficient (i.e. towards the bed) are less clear. With the possible exception of the curve for the smallest gap ratio, it would appear that the magnitude of negative C_L rises to a maximum and then falls with increasing Reynolds number.

In figure 7, the experimental results shown are those for the oscillating-tray rig for Reynolds numbers up to 2000 and for the pendulum rig at higher Reynolds numbers. The pendulum rig was found to be more reliable at high Reynolds numbers but less so at low Reynolds numbers. A comparison of the curves obtained in the two rigs when $U_0 D/\nu = 1500$ will be found in figure 9, below.

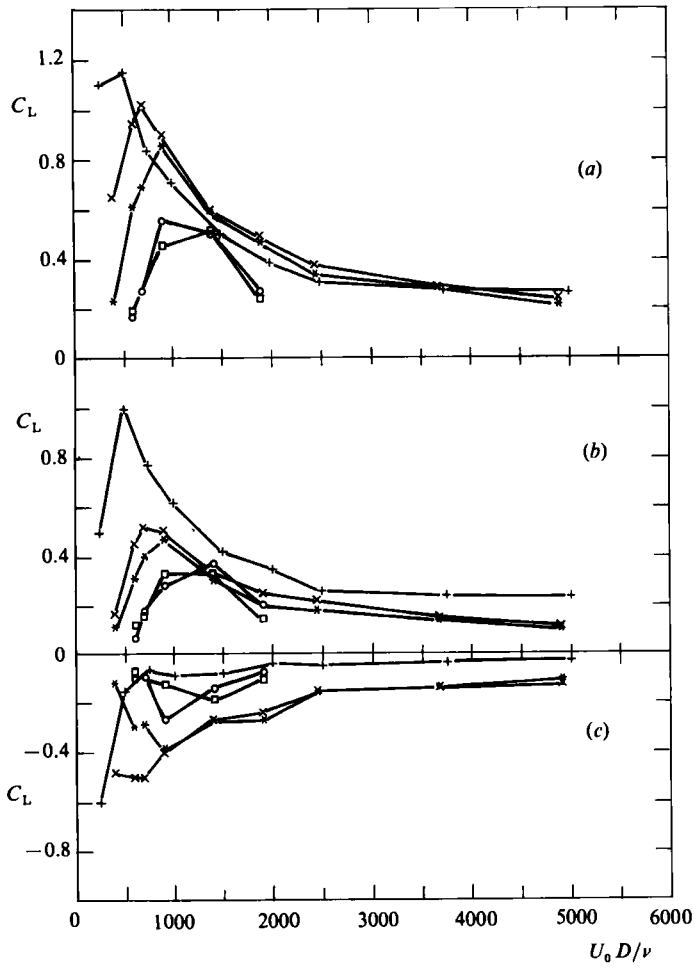

FIGURE 7. Variation with Reynolds number and gap ratio of (*a*) amplitude of the fluctuating lift coefficient; (*b*) maximum positive lift coefficient; (*c*) maximum negative lift coefficient. In all cases the bed was smooth and $\beta D = 14.0$. Values of ϵ/D are: +——+, 0.0156; ×——×, 0.25; *——*, 0.375; ⊙——⊙, 1.0; □——□, 1.5.

Figure 8 shows the corresponding results for $\beta D = 8.3$ and $\beta D = 4.2$. Although there is more experimental scatter, particularly at $\beta D = 4.2$, the curves are generally similar to those in figure 7. However, these curves do not show a clear maximum for C_L, possibly because they do not extend to low enough Reynolds numbers.

Figure 9 shows how the amplitude of C_L varies with ϵ/D for $\beta D = 14$. All that is clear is that the measurements do not follow the curve for potential flow (Milne Thomson 1968; Naheer 1977) although the trend of the curves as Reynolds number decreases suggests that agreement might possibly be better at lower Reynolds numbers. However, the reasonable agreement between the curves at $U_0 D/\nu = 1500$ for the oscillating-tray and the pendulum rigs is encouraging.

As stated in the Introduction, one of the motivations for the present study was the possible importance of lift for sediment transport. It is clear from figure 8 that, at least over some of the experimental range, the measured values of C_L are comparable to or even greater than typically quoted values of the drag coefficient

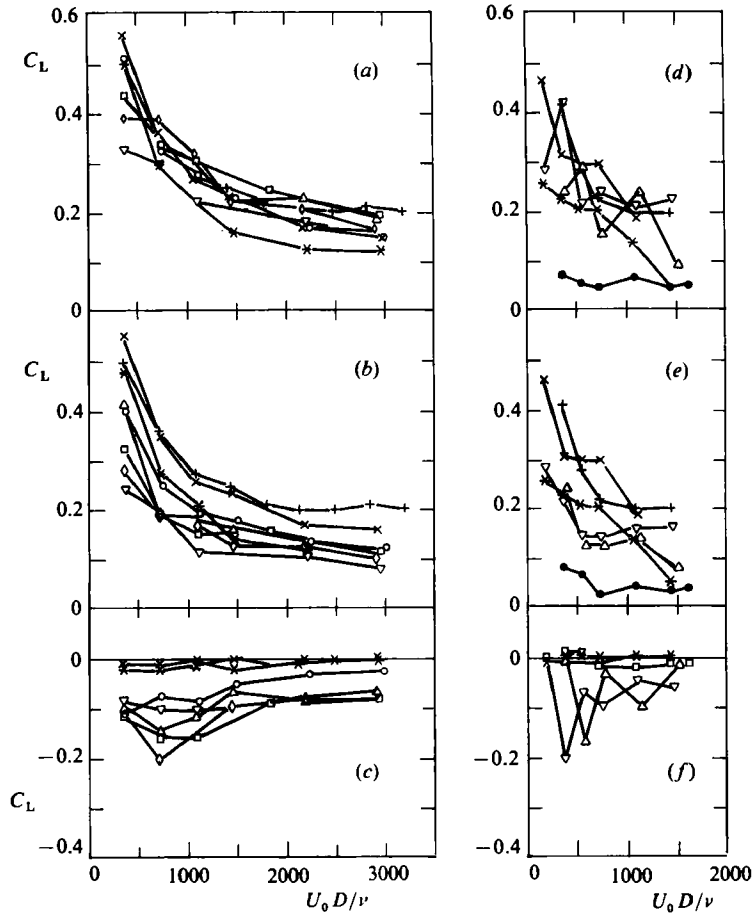

FIGURE 8. Variation of lift coefficient with Reynolds number and gap ratio for the smooth bed: (*a*) amplitude of the fluctuating lift coefficient for $\beta D = 8.3$; (*b*) maximum positive value of C_L for $\beta D = 8.3$; (*c*) maximum negative value of C_L for $\beta D = 8.3$; (*d*), (*e*), (*f*) as (*a*), (*b*), (*c*) respectively, except that $\beta D = 4.2$. Values of ϵ/D are: +——+, 0.0156; ×——×, 0.0312; *——*, 0.0625: ⊙——⊙, 0.125; □——□, 0.188; △——△, 0.25; ◇——◇, 0.375; ▽——▽, 0.5; ●——●, 1.0.

for flows of this sort. Of course, values of $\beta D = 4.2$ and 8.3 would only be found on site with very coarse sand or gravel. However, although for reasons of space it is not possible to present all of the experimental results here, it may be mentioned that similar values of C_L were also obtained for the smallest spheres tested ($\beta D = 1.33$). Further experimental results are given by Rosenthal (1986).

In figures 7, 8 and 9 the experimental results represent the average of the respective peaks in the two half-cycles and of several separate cycles. For the two larger values of βD the average of several cycles was adopted only to reduce experimental scatter. However, for $\beta D = 4.2$ it was clear from the records that the flow itself was unstable at larger Reynolds numbers. To quantify this effect the mean and standard deviation of the amplitude of the lift were calculated for a number of single cycles. Figure 10 shows how the standard deviation (s.d.) varies with βD and $U_0 D/\nu$ for one value of the gap ratio. Since the number of single cycles analysed in each case was small, usually not more than 10, there is considerable scatter. Nevertheless, it does look for the two smallest values of βD as if there is a critical condition beyond which the flow

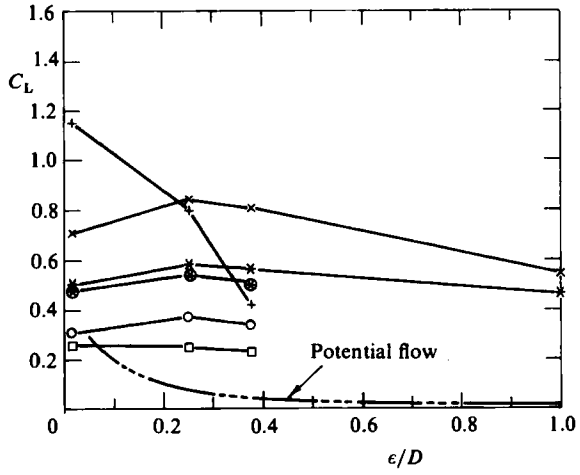

FIGURE 9. Variation of the amplitude of C_L with gap ratio for the smooth bed and $\beta D = 14.0$. For the oscillating tray values of $U_0 D/\nu$ are: +——+, 500; ×——×, 1000; *——*, 1500. For the pendulum rig values of $U_0 D/\nu$ are: ⊗——⊗, 1500; ⊙——⊙, 2500; □——□, 4500.

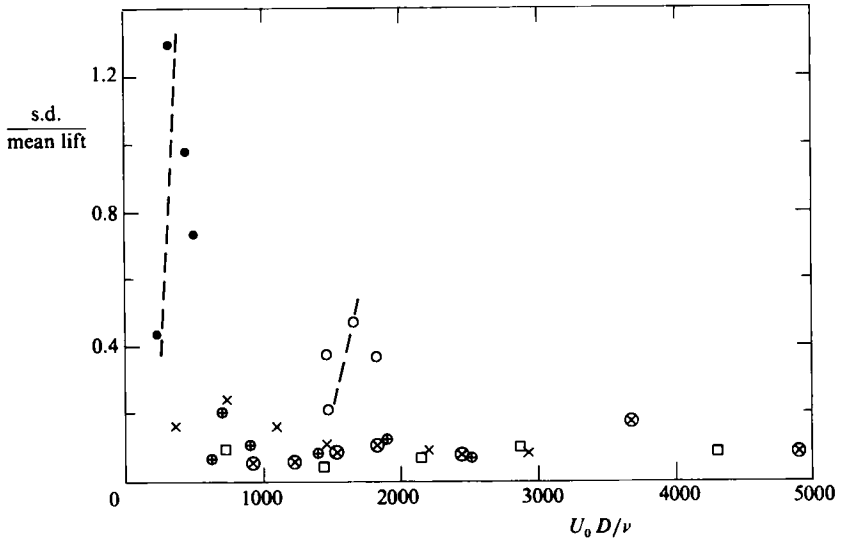

FIGURE 10. Variation with Reynolds number of the fluctuation in lift amplitude from cycle to cycle in the pendulum rig at $\epsilon/D = 0.25$. Values of βD are: ●, 1.33; ○, 4.2; ×, 8.3; ⊗, 14.0; □, 16.6; ⊕, 18.0.

becomes increasingly unstable. If the dashed curves are extrapolated back to the axis we obtain a critical Keulegan–Carpenter number $U_0 T/D$ approximately equal to 244 in each case. None of the experiments with the larger values of βD reached a Keulegan–Carpenter number as high as this although, if, as seems likely, the unsteadiness is associated with transition from laminar to turbulent flow, Keulegan–Carpenter number is probably not the controlling parameter over a very wide range of βD. Unfortunately, it was not possible with the present apparatus to investigate this question more fully.

So far, we have discussed only the peak values of the lift coefficient. It is also

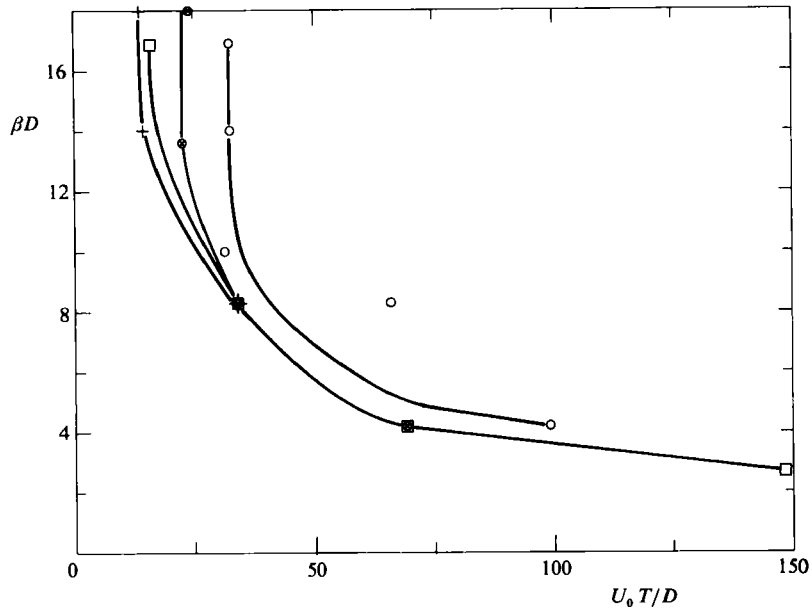

FIGURE 11. Values of $U_0 T/D$ at which, for various βD and ϵ/D, the spike was first clearly apparent in the lift record. Values of ϵ/D are: ○——○, 0.016; □——□, 0.063; +——+, 0.25; ⊗——⊗, 1.0.

interesting to examine the way in which C_L varies during the course of the cycle. Figure 5(*a*) shows that at sufficiently low Reynolds numbers the lift record is regular with peaks near the instant of maximum velocity (phase = $\frac{1}{2}\pi$, $\frac{3}{2}\pi$) and minima near the moment of zero velocity (phase = $0, \pi$). This is qualitatively similar to the variation in C_L with time predicted by potential-flow theory, although, as pointed out above, the amplitude of the fluctuation in C_L is significantly different. However, as Reynolds number increases we see the appearance in figure 5 of a subsidiary peak, or peaks, near the point at which the velocity reverses. In what follows, this subsidiary peak will be referred to as the 'spike'. Figure 11 shows the conditions under which the spike first begins to show clearly in the lift record. Because the lift signal becomes progressively more noisy as Reynolds number decreases, it is possible that the spike might occur at lower Reynolds numbers without being detected. Consequently, the curves in figure 11 should be taken as a rough indication only.

The most likely explanation for the spike is that it is associated with vortex formation around the sphere. As the flow reverses and the lee vortex is swept back round the sphere one would expect considerable perturbation of the flow. It should be admitted, however, that despite considerable efforts it did not prove possible to demonstrate this effect by flow visualization. The main problem was that oscillatory-flow patterns change so rapidly that it was difficult to be certain whether any particular feature was significant or not. This point is discussed further in §4.

Vortex formation in oscillatory flow depends both on Reynolds number and Keulegan–Carpenter number. At the largest value of βD the values of $U_0 D/\nu$ at which the spike was first detected were all greater than 1000. Since recirculating eddies appear behind an isolated sphere in steady flow for $U_0 D/\nu > 24$, it would seem that, if vortex formation is responsible for the spike, the controlling parameter must be $U_0 T/D$ rather than Reynolds number at these large values of βD. The curves in

figure 11 do indeed appear to tend towards a constant value of $U_0 T/D$ as βD increases, although the limiting values of Keulegan–Carpenter number are larger than those at which one would expect the first signs of vortex formation. For example Carstens (1952) observed signs of vortex formation at large βD when $U_0 T/D > 3.1$. They are, however, within the range for which vortex formation is known to affect the results for the in-line force (see, e.g., Sarpkaya 1975). At smaller values of βD viscous effects are relatively more important and consequently the appearance of the spike is not controlled by $U_0 T/D$ alone. At extremely low βD we might expect Reynolds number (based on local velocity) to be dominant but the present results do not extend far enough to test that hypothesis.

The curves in figure 11 seem to indicate that for any given βD the spike appears first for intermediate values of the gap ratio ϵ/D. If, as suggested above, the spike is associated with asymmetry in vortex formation and ejection, the reduction at large ϵ/D is to be expected. It is less clear why the spike should be inhibited when the sphere is very close to the wall.

3.2. *Rough bed*

Figure 12 shows how the maximum positive lift, maximum negative lift, and amplitude of the lift coefficient vary with Reynolds number and gap ratio for two rough beds. The flow conditions were the same as those for the smooth-bed results shown in figure 8. However, when comparing the two sets of results it has to be borne in mind that the gap ratio ϵ/D does not have quite the same significance. In both cases ϵ is the distance of the bottom of the sphere above the surface of the tray. Thus, for $\epsilon/D = 0$ the sphere in the smooth-bed tests would be touching the surface of the tray but otherwise completely exposed to the flow, whereas in the rough-bed tests the sphere is shielded by similar spheres at the same level. Thus, it is hardly surprising that the values of C_L in figure 12 should be generally less than the corresponding values in figure 8. Otherwise, the trends are similar.

For the results shown in figure 12 there was a gap under the sphere for values of ϵ/D greater than zero. Clearly, this gap might affect the measured lift, particularly for large values of ϵ/D. Figure 13 shows the effect of different methods of mounting the sphere when $\epsilon/D = 1.0$. The results are for three different arrangements. The first corresponds to the conditions of figure 12, i.e. no attempt to fill the void under the raised sphere. (This is called arrangement A in figure 13.) In the second arrangement (arrangement B) a dummy sphere was placed directly under the test sphere. The rod from the transducer to the test sphere passed through a hole drilled through the middle of this sphere. The third arrangement (C) was with the bed completely packed with spheres and the support rod from the transducer passing through the gap between three adjacent spheres. The test sphere was thus above a hollow in the bed. It would appear from figure 13 that the measured lift is strongly dependent on the method of mounting, particularly at low Reynolds numbers. At smaller values of ϵ/D the void under the sphere is not so exposed to the flow and consequently its effect may be less significant.

4. Comparison with other work

As far as the authors are aware, the only other measurements of lift on spherical particles in oscillating flow are those contained in an unpublished thesis by Sert (1977). These measurements were made in a laboratory wave channel and cover the range $5.5 < \beta D < 10.0$ and $28 < U_0 D/\nu < 540$. Unfortunately, there is some evidence

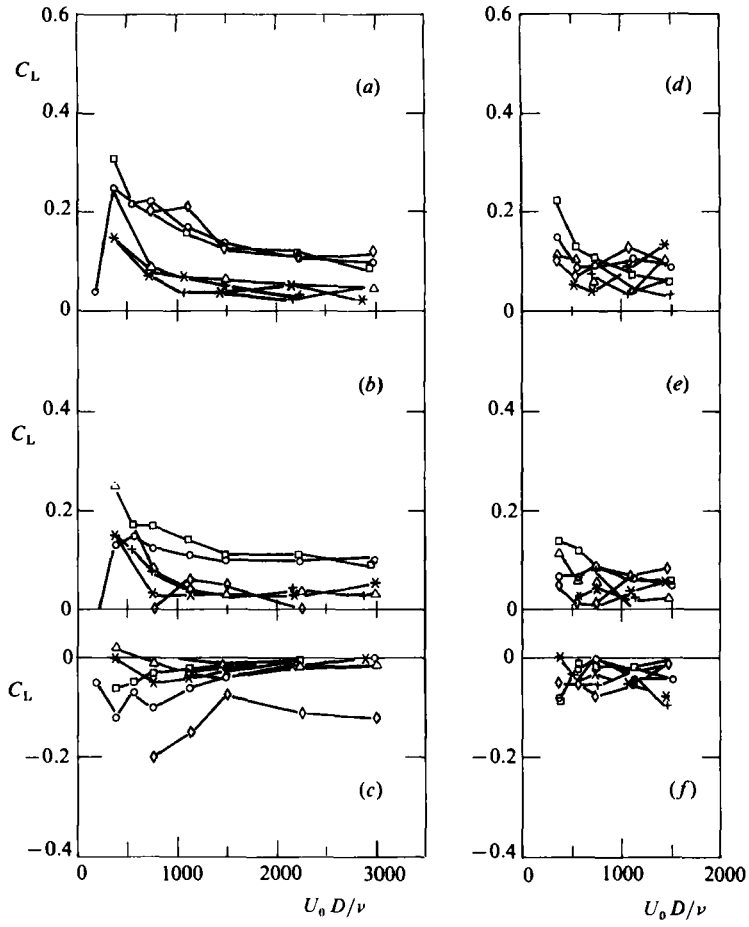

FIGURE 12. Variation of lift coefficient with Reynolds number and gap ratio for the rough bed: (*a*) amplitude of the fluctuating lift coefficient for $\beta D = 8.3$; (*b*) maximum positive value of C_L for $\beta D = 8.3$; (*c*) maximum negative value of C_L for $\beta D = 8.3$; (*d*), (*e*), (*f*) as (*a*), (*b*), (*c*) respectively, except that $\beta D = 4.2$. Values of ϵ/D are: +——+, 0.0078 ($\beta D = 8.3$), 0.0312 ($\beta D = 4.2$); ×——×, 0.0625; *——*, 0.125; ○——○, 0.25; □——□, 0.5; △——△, 0.75; ◇——◇, 1.0.

to suggest that Sert's 'lift' signal was affected by the drag force on the sphere. In particular, the time variation of the 'lift' signal is generally similar to that of the drag (one peak per cycle) whereas, on grounds of symmetry, one would expect it to be almost the same from one half-cycle to the next (two peaks per cycle). For the records reproduced in Sert's thesis the difference in fluid velocity near the bed during the two half-cycles would have been less than 5%, which is too small to account for the anomaly in the lift record. Nevertheless, the general trend of Sert's results is similar to that of the present tests: the amplitude of C_L falls steadily with increasing Reynolds number as shown in figures 8 and 12. However, in the restricted range of Reynolds numbers for which the two sets of tests overlap the values of C_L which Sert obtained are approximately twice those shown here.

There have been many lift measurements for spheres in steady flow. Those of Davies & Samad (1978) cover a similar range of Reynolds numbers to the present study. In their tests, only spheres actually touching a plane wall were examined. Bearing in

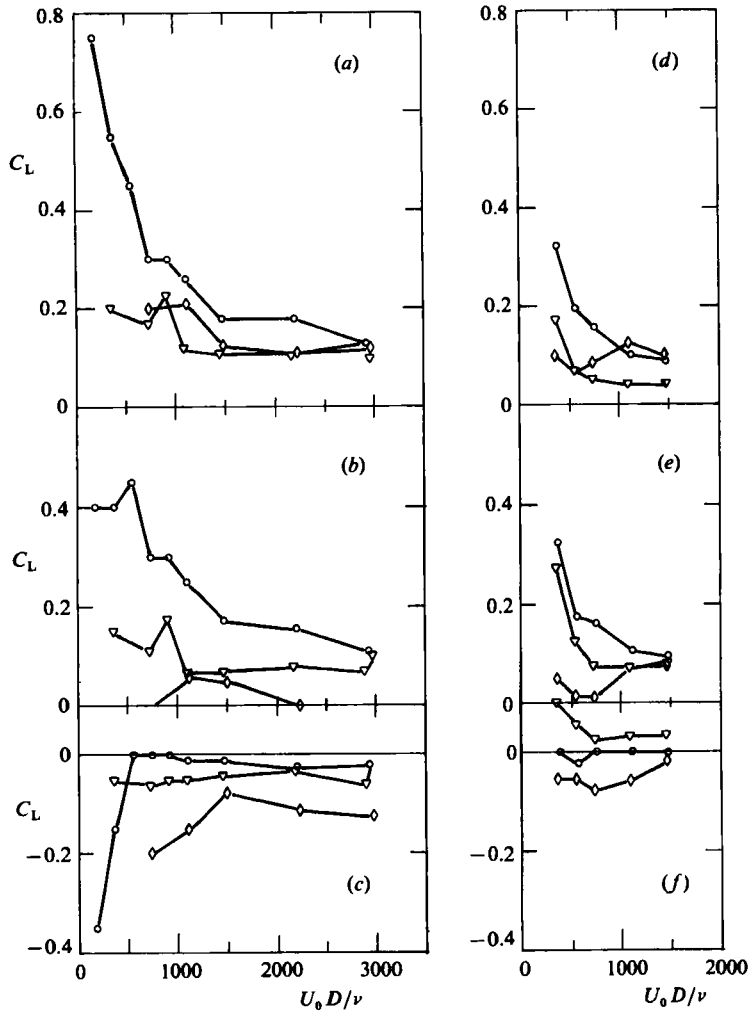

FIGURE 13. Comparison of different methods of mounting the sphere for the rough bed at $\epsilon/D = 1.0$: (*a*) amplitude of fluctuating lift coefficient at $\beta D = 8.3$; (*b*) maximum value of C_L at $\beta D = 8.3$; (*c*) maximum negative value of C_L at $\beta D = 8.3$; (*d*), (*e*), (*f*) as (*a*), (*b*), (*c*) respectively, except that $\beta D = 4.2$. Symbols are: ◇——◇, arrangement A; ○——○, arrangement B; ▽——▽, arrangement C.

mind the considerable experimental scatter, the values of C_L which they obtained are generally similar to those in the present tests with the smallest gap ratio. Measurements of lift for varying gap ratio have been made by various investigators (see Willetts & Murray 1981). Although the range of C_L values shown by those tests is similar to that in the present tests the variation in C_L with ϵ/D is significantly different. One reason for this disagreement may be that the Reynolds numbers in the steady-flow tests were much greater than in the present study. A second reason is that velocity profiles in oscillatory flow are different from those in steady flow.

It is also of interest to compare the present results with those for cylinders in oscillatory flow. Sarpkaya (1976) found that at very low values of the Keulegan–Carpenter number U_0T/D both positive lift (i.e. away from the wall) and negative lift (towards the wall) tended to zero. As U_0T/D increased, both positive and negative

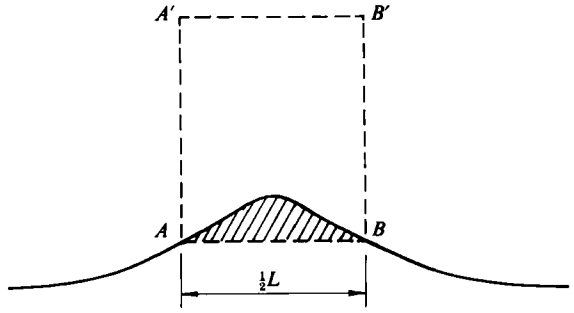

FIGURE 14. Bed profile for lift computations.

C_L increased to maxima and then decreased. In figure 7, D is constant and T and ν are nearly so and consequently $U_0 D/\nu$ is approximately proportional to Keulegan–Carpenter number. Thus the trends observed by Sarpkaya are similar to those shown in figure 7.

Further insight into the present test results may be obtained by comparison with numerical computations for two-dimensional bodies in oscillatory flow. Sleath (1973) put forward a finite-difference time-marching method for rippled beds and Du Toit & Sleath (1981) have compared the predictions of this model with direct measurements of the fluid velocities. It is easy to apply these results to calculate the lift on a segment of bed such as the shaded area shown in figure 14. Clearly, the lift per unit width on the shaded portion of bed is

$$\text{lift} = -\rho \frac{\partial}{\partial t} \iint v \, \mathrm{d}x \, \mathrm{d}y + \int_A^{A'} \rho uv \, \mathrm{d}y - \int_B^{B'} \rho uv \, \mathrm{d}y,$$

where u and v are the horizontal and vertical components of fluid velocity and the double integral applies to all of the fluid within the dashed control surface shown in figure 14. The upper boundary $A'B'$ of this control surface is assumed to be at infinity. Making use of Sleath's numerical computations of velocity we obtain, for $\beta \frac{1}{2}L = 15$, the curves shown in figure 15. In this figure the lift coefficient is defined as

$$C_L = \frac{\text{lift per unit width}}{\frac{1}{2}\rho U_0^2 \frac{1}{2}L},$$

where L is the ripple wavelength.

The first thing we note is that the general shape of the curves in figure 15(*d–f*), for the amplitude of the fluctuating lift coefficient and its maximum positive and negative values, is similar to that of the corresponding curves in figure 7. The variation in C_L during the course of the cycle, shown by figure 15(*a–c*), is also generally similar to that in figure 5. At sufficiently low values of $U_0 L/2\nu$ the variation of C_L with time is almost sinusoidal but at higher values a secondary peak begins to appear in the lift record. The fact that the secondary peak occurs somewhat earlier in the cycle in figure 15(*c*) than in figure 5 may be due to the relatively deeper immersion of the ripple in the viscous boundary layer with consequently earlier local flow reversal.

For this two-dimensional bed, vortex formation first occurs at a value of $U_0 L/2\nu$ of about 600. This is also approximately the point at which the C_L *versus* Reynolds-number curves in figures 15(*d*, *e*) reach their maxima. However, the spike in the lift record is not clearly marked until significantly higher Reynolds numbers. Figure 15(*b*)

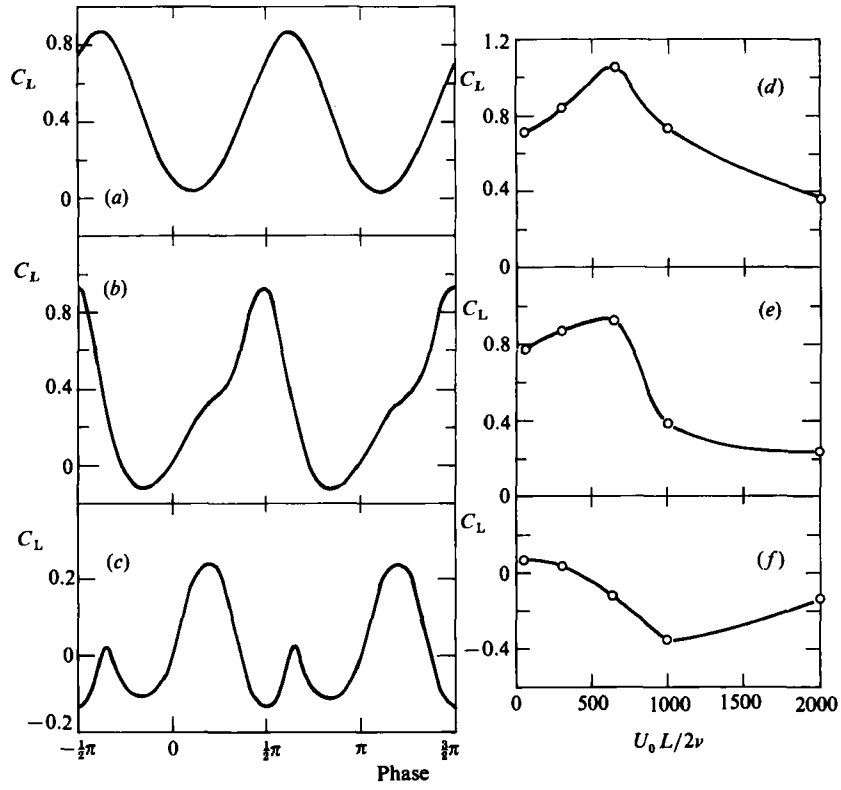

FIGURE 15. Computed lift coefficients for $\beta\frac{1}{2}L = 15.0$. (*a*), (*b*), (*c*): examples of the way in which C_L varies during the course of the cycle for $U_0 L/2\nu = 300$, 640, 2000, respectively. (*d*), (*e*), (*f*): variation with Reynolds number of, respectively, amplitude of fluctuating C_L, maximum positive C_L, maximum negative C_L.

shows that although the lift record at $U_0 L/2\nu = 640$ is no longer sinusoidal it does not yet have a secondary peak.

Although the two-dimensional profile shown in figure 14 is very different from a sphere close to a plane bed, it seems reasonable to draw the following tentative conclusions from this comparison. Firstly, the maximum in the C_L *versus* Reynolds-number curves in figure 7 probably occurs near the point at which vortices begin to form. Secondly, the spike in the lift record in figure 5 is probably associated with vortex formation but does not show clearly until significantly higher Reynolds numbers than those at which vortices begin to form.

No attempt will be made to compare the present experimental results with Saffman's (1965) theoretical expression for a sphere in a shear flow. All of the spheres tested were relatively large compared with the viscous-boundary-layer lengthscale $1/\beta$. Consequently, the flow to which they were exposed did not even approximate to a uniform shear flow. Also, the Reynolds numbers were much larger than those to which Saffman's expression is supposed to apply.

5. Conclusions

(i) Measurements have been made of the lift on a sphere in oscillatory flow close to both smooth and rough beds using two different rigs. One consisted of a tray oscillated by a motor and the other of a free-swinging tray suspended from the roof.

(ii) At sufficiently low Reynolds numbers the maximum lift occurs near the point at which velocity is maximum and the minimum lift near velocity reversal. At higher Reynolds numbers a secondary peak appears near the point of velocity reversal.

(iii) It is suggested that this secondary peak is associated with vortex formation around the sphere.

(iv) The lift-coefficient *versus* Reynolds-number curves all showed a somewhat similar pattern. When the sphere diameter D was large compared with the viscous-boundary-layer lengthscale $1/\beta$ $(= (2\nu/\omega)^{\frac{1}{2}})$, the amplitude and maximum positive values of C_L initially increased with increasing Reynolds number, reached a maximum, and then progressively decreased. At smaller βD, measurements were not extended to sufficiently low Reynolds numbers to show the initial rise but otherwise the shape of the curves was similar. Numerical computations for two-dimensional roughness suggested that the maximum is found near the point at which vortex formation first occurs.

(v) For the two smallest values of βD the lift record became unstable when the Keulegan–Carpenter number exceeded approximately 244. For the larger values of βD no significant instability was observed.

(vi) Tests were carried out for $180 < U_0 D/\nu < 6000$ and for $1.3 < \beta D < 18$. Even at the lowest values of βD the lift coefficient was far from negligible compared with typically quoted values of the drag coefficient. This would suggest that lift may be more important for the transport of coarse sediment in oscillatory flow than has previously been realized. If this is so, current attempts to model wave-induced sediment transport with the aid of formulae derived for steady flow may be of limited value. This is clearly a question which requires further investigation.

REFERENCES

Aksoy, S. 1973 Fluid force acting on a sphere near a solid boundary. In *Proc. 15th IAHR Cong., Istanbul*, pp. 217–224.

Auton, T. R. 1984 The dynamics of bubbles, drops and particles in motion in liquids. Ph.D. dissertation, Cambridge University.

Bagnold, R. A. 1974 Fluid forces on a body in shear flow; experimental use of stationary flow. *Proc. R. Soc. Lond.* A **340**, 147–171.

Carstens, M. R. 1952 Accelerated motion of a spherical particle. *Trans. Am. Geophys. Union* **33**, 713–721.

Chen, C. & Carstens, M. R. 1973 Mechanics of removal of a spherical particle from a flat bed. In *Proc. 15th IAHR Cong., Istanbul*, pp. 147–158.

Chepil, W. S. 1961 The use of spheres to measure lift and drag on wind-eroded soil grains. *Proc. Soil Sci. Soc.* **5**, 343.

Coleman, N. L. 1967 A theoretical and experimental study of drag and lift forces acting on a sphere resting on a hypothetical streambed. In *Proc. 12th Congress IAHR Fort Collins*, pp. 185–192.

Davies, T. R. H. & Samad, M. F. A. 1978 Fluid dynamic lift on a bed particle. *Proc. ASCE J. Hydraul. Div.* **104**, 1171–1182.

Du Toit, C. G. & Sleath, J. F. A. 1981 Velocity measurements close to rippled beds in oscillatory flow. *J. Fluid Mech.* **112**, 71–96.

LEE, K. C. 1979 Aerodynamic interaction between two spheres at Reynolds numbers around 10^4. *Aero. Q.* **15**, 371–385.

MAULL, D. J. & MILLINER, M. G. 1978 Forces on a circular cylinder having a complex periodic motion. In *Mechanics of Wave-Induced Forces on Cylinders* (ed. T. L. Shaw), pp. 490–502. Fearon Pitman.

MAULL, D. J. & NORMAN, S. J. 1978 A horizontal circular cylinder under waves. In *Mechanics of Wave-Induced Forces on Cylinders* (ed. T. L. Shaw), pp. 359–378. Fearon Pitman.

MILNE THOMSON, L. M. 1968 *Theoretical Hydrodynamics*. 5th edn. Macmillan.

NAHEER, E. 1977 Stability of bottom armoring under the attack of solitary waves. *Calif. Inst. of Tech. W. M. Keck Lab. Rep.* Kh-R-34.

ROSENTHAL, G. N. 1986 Lift forces on spherical particles near a horizontal bed in oscillatory flow. Ph.D. dissertation, Cambridge University.

RUBINOW, S. I. & KELLER, J. B. 1961 The transverse force on a spinning sphere moving in a viscous fluid. *J. Fluid Mech.* **11**, 447–459.

SAFFMAN, P. G. 1965 The lift on a small sphere in a slow shear flow. *J. Fluid Mech.* **22**, 385–400 (and Corrigendum **31** (1968), 624).

SARPKAYA, T. 1975 Forces on cylinders and spheres in a sinusoidally oscillating fluid. *Trans. ASME* E: *J. Appl. Mech.* **42**, 32–37.

SARPKAYA, T. 1976 Forces on cylinders near a plane boundary in a sinusoidally oscillating fluid. *Trans. ASME* I: *J. Fluids Engng* **98**, 499–505.

SERT, M. 1977 The force on a particle near a bed acted upon by water waves. Ph.D. dissertation, Cambridge University.

SLEATH, J. F. A. 1973 A numerical study of the influence of bottom roughness on mass transport by water waves. In *Numerical Methods in Fluid Dynamics* (ed. C. A. Brebbia and J. J. Connor). Pentech Press.

SWANSON, W. M. 1961 The Magnus effect: a summary of investigations to date. *Trans. ASME* D: *J. Basic Engng* **83**, 461–470.

THOMSCHKE, H. 1971 Experimentelle Untersuchung der stationären Umströmung von Kugel und Zylinder in Wandnähe. Doctoral thesis, Karlsruhe University.

WILLETTS, B. B. & MURRAY, C. G. 1981 Lift exerted on stationary spheres in turbulent flow. *J. Fluid Mech.* **105**, 487–505.

WILLMARTH, W. W. & ENLOW, R. L. 1969 Aerodynamic lift and moment fluctuations of a sphere. *J. Fluid Mech.* **36**, 417–432.

YOUNG, D. F. 1960 Drag and lift on spheres within cylindrical tubes. *Proc. ASCE J. Hydraul. Div.* **86**, 47.